Per-pixel unmixing of spectrally overlapping fluorophores using intra-exposure excitation modulation

Hana Valenta[1], Franziska Bierbuesse[1], Raffaele Vitale[2], Cyril Ruckebusch[2], Wim Vandenberg[1], Peter Dedecker[1]

[1] Department of Chemistry, KU Leuven, Belgium
[2] LASIRE CNRS, University of Lille, France

peter.dedecker@kuleuven.be

April 29, 2023

Abstract

Multilabel fluorescence imaging is essential for the visualization of complex systems, though a major challenge is the limited width of the usable spectral window. Here, we present a new method, exNEEMO, enabling per-pixel unmixing of spectrally-overlapping fluorophores based on their light-induced dynamics, in a way that is compatible with a very broad range of timescales over which these dynamics may occur. Our approach makes use of non-negative least squares projection to decompose the observed emission given the reference responses of the individual fluorophores that are present in the sample. We apply the approach to the simultaneous of four green photochromic fluorescent proteins, allowing us to visualize the distribution of each fluorophore at the full resolution of the imaging. Our methodology opens new possibilities for the multiplexing of fluorescence imaging.

Introduction

Fluorescence microscopy is a key technology in the life sciences, though it is limited in the number of components that can be visualized at once. Several solutions to address this limitation have been developed, including computational approaches based on spectral unmixing or the use of fluorescence properties other than the emission color, such as fluorescence anisotropy [1], fluorescence lifetime [2], or light-induced processes resulting in characteristic fluorescence dynamics in the emission [3, 4, 5, 6].

We recently developed intra-exposure excitation modulation (NEEMO), a method that can distinguish multiple spectrally-identical fluorophores based on differences in their light-induced fluorescence dynamics, in a way that can recognize such dynamics over a broad range of timescales [7]. Using this approach, we were able to distinguish the fast light-induced fluorescence dynamics of four spectrally-identical reversibly photoswitchable fluorescent proteins (rsFPs) expressed within *E. coli* bacteria. Such labels can be controllably switched between a fluorescent and a non-fluorescent state using illumination at two different wavelengths. This previous work focused on the classification of cells expressing just one of these fluorophores rather than separating the contributions of each fluorophore within (potentially complex) mixtures. Such classifications are easier to achieve since the signal can be averaged over the entire cell geometry, leading to much better signal-to-noise ratios, while the analysis can be based on clustering approaches that are tolerant to slight changes in label behavior as long as each cell can still be assigned to the correct cluster. Such an approach has also been used, for example, to discrimate up to 9 among 16 spectrally similar fluorophores in bacteria using a method called LIGHTNING [8].

The true quantitative separation of fluorophores within complex mixtures has also seen multiple efforts over the past years, resulting in approaches such as OLID, SAFIRe, OPIOM, and HIGHLIGHT [9, 10, 11, 12, 8, 13], though these methods require that the different fluorescence dynamics can be directly resolved by the microscope, which may be challenging if the detection is done using a camera that is typically much slower compared to the point detectors used in confocal imaging.

In this manuscript, we explored whether the NEEMO concept can be extended to provide true quantitative emitter separation, in a manner that takes advantage of the full spatial resolution of the imaging, while still being capable of resolving fast fluorescence dynamics. Here, we present the extended NEEMO (exNEEMO) method demonstrating the per-pixel unmixing of four spectrally identical rsFPs expressed simultaneously in eukaryotic cells based on their unique photoswitching profiles, while requiring the acquisition of just four fluorescence images. We find that this method yields a reasonable performance and delivers compatibility with a broad range of fluorescence dynamics, though the overall accuracy is limited by cell-to-cell variations in the photoswitching dynamics of the labels. In doing so, the method enables new dimensions for multiplexed fluorescence imaging of complex biological systems.

Results and discussion

We start by briefly revisiting the principle underlying our method, schematically shown in Figure 1A. The core idea is that different photoswitching efficiencies of the fluorophores result in faster or slower responses to modulation of the excitation light. As a result, the fluorescence emitted by each type of fluorophore displays a characteristic response profile to temporally-varying illumination with the on- and off-switching light. In NEEMO, we do not detect these responses directly but instead measure only their integrated emission over the camera exposure time. The different labels can then be identified by observing how the integrated intensities vary for different illumination patterns [7]. This approach is compatible with a very broad range of fluorescence dynamics since these dynamics do not need to be resolved by the imaging system directly, but require only that they can be probed within the modulation rate of the light sources, which is typically very fast (within microseconds or faster) even for inexpensive systems.

In our previous study, two to four images with different excitation light modulations were sufficient to classify four different types of fluorophores according to their fluorescence dynamics [7]. To quantitatively separate mixtures, the number of acquired images must at least be equal to the number of components in the mixture. To test this approach in practice, we expressed these fluorophores in HeLa cells using different targeting motifs for each label. In particular, we targeted EGFP to the plasma membrane, ffDronpa to the nucleus, ffDronpaF to vimentin and ffDronpa2F to the peroxisomes. Exposing cells that expressed just one of these fluorophores to the modulation pattern shown in Figure 1B revealed both distinct localization patterns and clearly different fluorescence responses (Figure 1C and Supplementary Movies S1-4)), reflecting the differences in photochromism efficiencies. To avoid possible bias in the cell selection, we repeated this procedure at randomly-selected positions in the sample, allowing the measurement of fluorescence reference profiles over many different cells (Figure 1D). While the overall trends in fluorescence intensities were consistent, this analysis did reveal noticeable cell-to-cell variability that also depended on the observed overall emission brightness. While most reference traces were well-defined and consistent, a minority displayed deviations largely for cells that displayed low brightnesses and were therefore difficult to analyze. It is also possible that additional variability is induced through the use of fixed cells [14].

These characteristic fluorophore responses were apparent also when imaging HeLa cells expressing all four labels simultaneously (Figure 2A and Supplementary Movie S5), though it is difficult to distinguish the four rsFPs in the measured images by eye. We instead analyzed these images using non-negative least squares projection [15]. In this approach, the measured image $\boldsymbol{D}$ is decomposed into the product of the local concentrations of each fluorophore $\boldsymbol{C}$ and the known responses of these fluorophores to the illumination ($\boldsymbol{S}$). Because the measurement is susceptible to noise, we must also include an error term $\boldsymbol{E}$ such that

$$\boldsymbol{D} = \boldsymbol{C}\boldsymbol{S}^{\boldsymbol{T}} + \boldsymbol{E} \tag{1}$$

The analysis then tries to solve this system of equations to determine $\boldsymbol{C}$ and $\boldsymbol{E}$. In our experiments, $\boldsymbol{D}$, $\boldsymbol{C}$, and $\boldsymbol{E}$ are of dimensions $N \times 4$, where N is the total number of pixels in a fluorescence image and $\boldsymbol{S}$ is a 4×4 matrix containing the responses of the fluorophores as determined from the single-fluorophore control measurements. The dimensions of this matrix arise because we have four different fluorophores and four different illumination patterns. To create $\boldsymbol{D}$, the four images acquired with different illumination patterns are simply unfolded by concatenating all of the pixel values from a given image into a one-dimensional vector. More information on the analysis is provided in the methods section of this work.

Figure 2B and C show an example result from this analysis. Using just the four images acquired using different illumination modulations, the contributions of the different fluorophores can be selectively extracted to reveal the structural features associated with the expected intracellular targeting. Figure 2B displays the

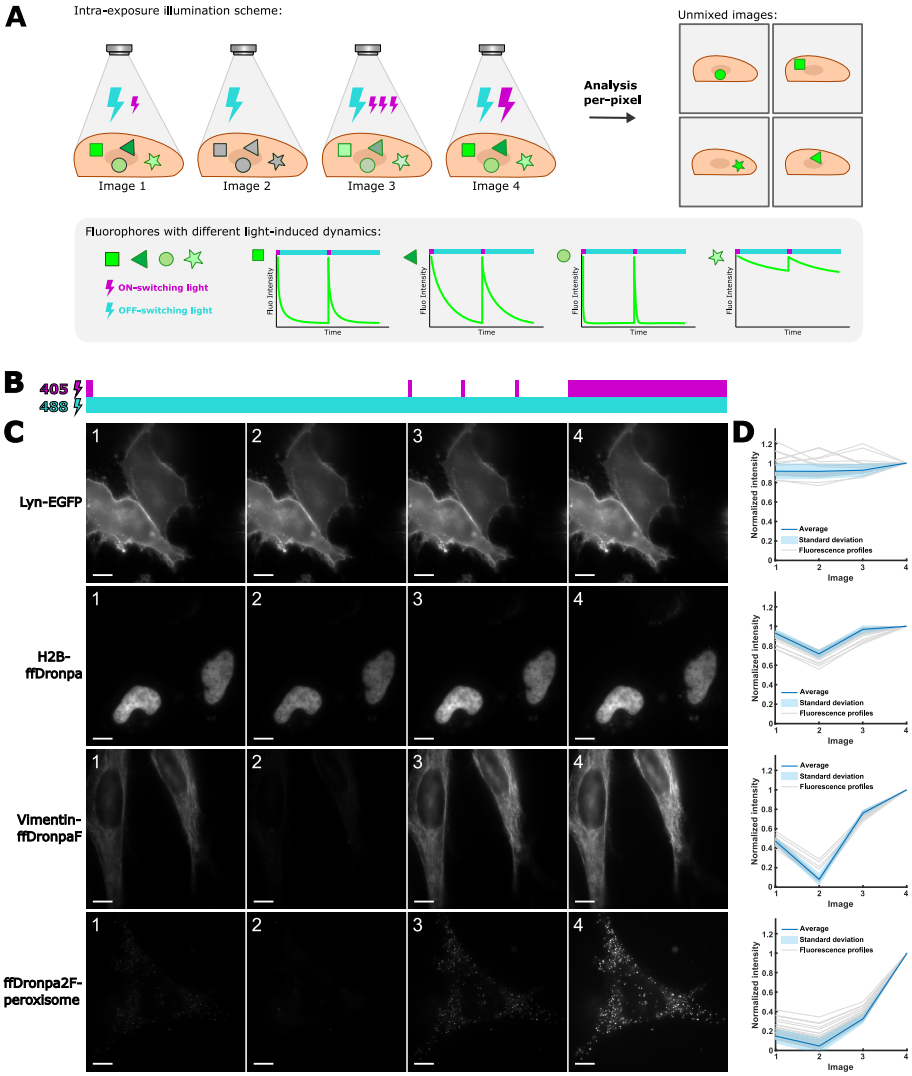

Figure 1: A: Concept of the exNEEMO method. B: Illumination patterns used to probe the distinct photochromism efficiencies and (C) resulting fluorescence images for representative fixed HeLa cells that expressed a single fluorophore (B). D: Fluorescence profiles (normalized to the fourth image) for all cells expressing single fluorophores. Each line shows a single distinct field of view where the color indicates the observed fluorescence brightness.

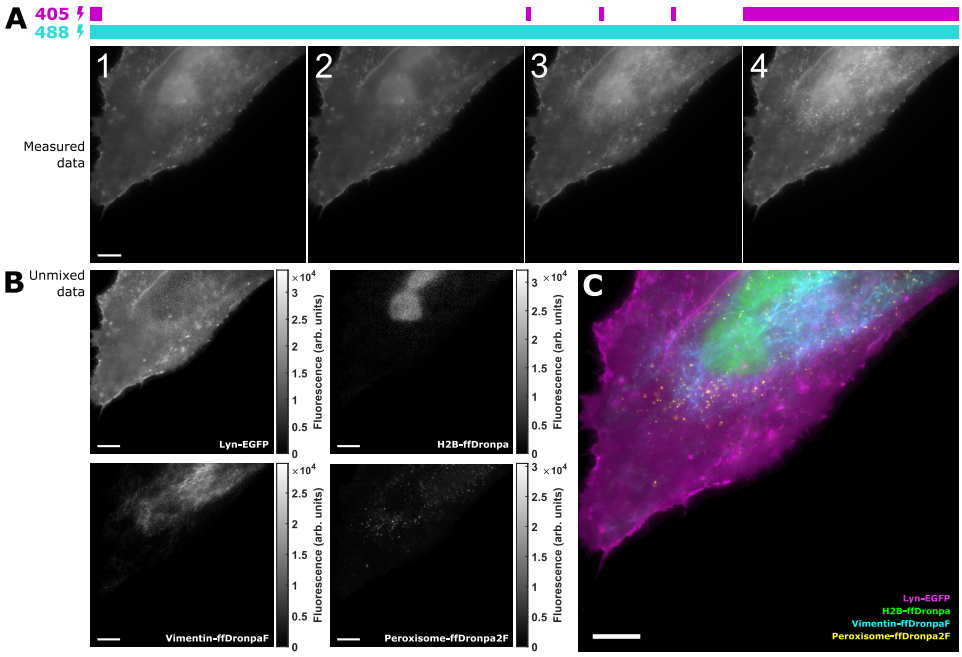

Figure 2: A: HeLa cells expressing all four rsFPs imaged under the specific illumination scheme of violet and cyan light, resulting in a four-image sequence. B: exNEEMO output - unmixed rsFPs revealing four different cell structures. C: Merge of unmixed false color images produced by exNEEMO. Scale bars 10 µm.

individual single-fluorophore images, making it possible to observe whether there is crosstalk between the different channels. Some crosstalk is observed between the EGFP and ffDronpa signal, manifesting as increased noise in the EGFP image, though the overall features are retained. Supplementary Figure S1 shows additional results obtained on a random selection of cells expressing these constructs.

A key goal was to evaluate the extent of the ambiguity or uncertainty in the analysis. Figure 3 visualizes the results of our analysis for cells expressing just one type of fluorophore. A visual inspection of example images indeed underscores a high degree of specificity within each of the detected channels (Figure 3A). To obtain unbiased results, we performed a quantitative analysis of the separation accuracies on multiple cells (84 cells distributed over 39 field-of-views for Lyn-EGFP, 83 cells distributed over 39 field-of-views for H2B-ffDronpa, 41 cells distributed over 22 field-of-views for vimentin-ffDronpaF and 84 cells distributed over 40 field-of-views for peroxisome-ffDronpa2F), by calculating the fluorescence brightness determined for each fluorophore for the fourth (brightest) fluorescence image (Figure 3B). These showed that on average about 80% to 90% of the signal was correctly assigned by the analysis.

The absolute contributions of each fluorophore are determined not only by the measured data but also by the absolute values of the reference profiles. In simplified terms, the analysis determines the weighted sum of the reference profiles that best describes the experimental data acquired in each detector pixel. Scaling the values of the reference profiles by a factor A therefore results in a reduction of the corresponding fluorophore contribution estimated by the analysis by the same factor A. In principle, the reference profiles could be scaled to match the relative brightnesses of each fluorophore, permitting direct comparison. If, however, the reference profiles are contaminated by the presence of background, meaning that there is an offset that is not removed, then the profile will tend to 'flatten out' and signal is likely to be spuriously assigned to the fluorophore that has the least modulation of its fluorescence.

In order to estimate to what extent signals might be unaccounted for or spuriously generated by our analysis, we calculated a residual image for the fourth fluorescence image, showing the difference between the calculated and measured fluorescence intensities (this is equivalent to the matrix $\boldsymbol{E}$ described in the methods section). Figure 3C visualizes these for the single-fluorophore data, showing that the magnitude of these residuals is within 10% of the observed fluorescence intensities, though non-accounted for sample structuring is visible for ffDronpaF and ffDronpa2F. We sought to understand whether this imperfect unmixing could arise from the variability in fluorophore response profiles observed between cells expressing the same construct, as was observed in Figure 1D. To do so, we calculated contribution plots similar to those in Figure 3B, but using not the averaged illumination response profiles but rather the response profiles observed for

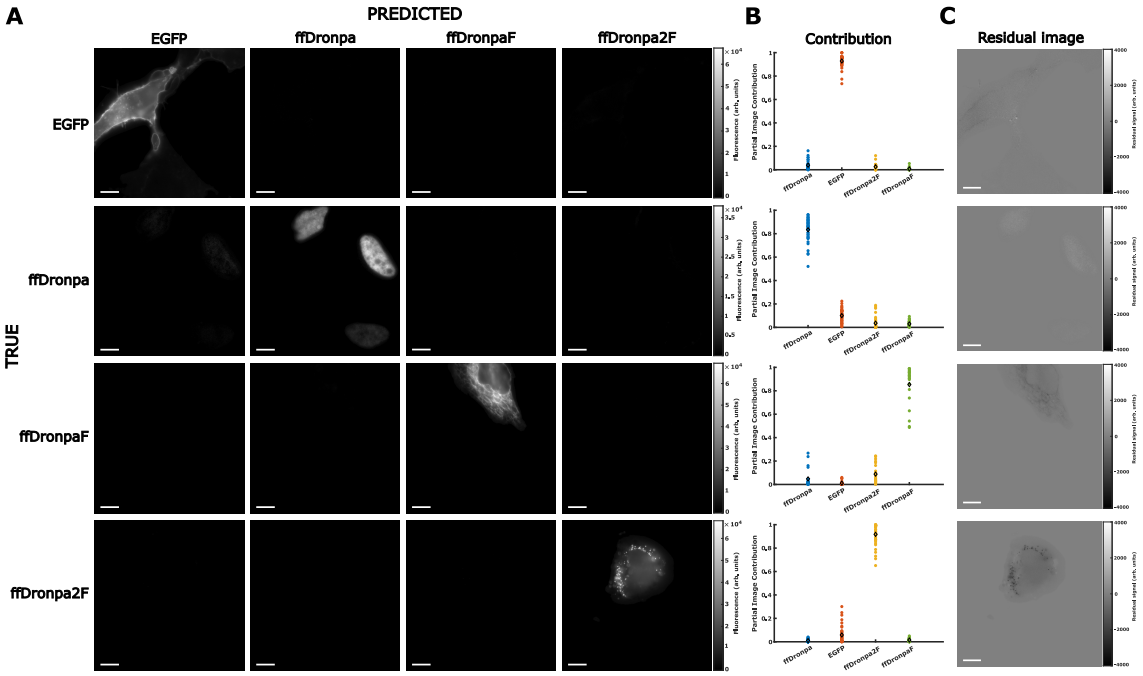

Figure 3: A: exNEEMO analysis of the cells expressing a single rsFP. B: Correctness of identification of each rsFP shown as contribution plots. One dot represent one image (FOV). The diamond sign represents the average. C: Residual images show residual signal when subtracting the image produced by the exNEEMO from the measured image. Contributions of all four components were used in the calculation of the residual images.

individual fields-of-view, applying this to all of the other cells in turn. Figure 4 shows an example of this for varying ffDronpa2F reference profiles, while Supplementary Figure S2 shows this data also when varying the reference profiles of the other fluorophores. We find that the choice of reference profile has an effect on the extracted contributions, but that the resulting variation is fairly small and associated with specific fields-of-view or strongly deviating reference profiles (Supplementary Figure S3). Such issues can be mitigated by applying even modest selection on the individual reference profiles included in as part of the analysis. Individual analyses can also be investigated using residual images similar to those shown in Figure 3C.

Conclusions

In this work, we have developed an approach for the spatially-resolved separation of mixtures of different emitters based on their light-induced fluorescence dynamics. The core idea is to illuminate the sample with temporally-varying light intensities, to which the fluorophores respond with characteristic emission profiles determined by nature of the illumination pattern and the kinetics of their fluorescence dynamics. Compared to other approaches, our method has the advantage that it can make use of fluorescence dynamics that occur too quickly to be resolved by the camera detector, but that are well within the rates at which even inexpensive light sources can be modulated.

Compared to our previous work, which was focused on the classification of samples expressing a single fluorophore each, the methodology in this work can resolve fluorophore mixtures down to the 'per pixel' limit in which the full spatial resolution of the imaging is retained. To do so, we assume that the characteristic fluorophore response profiles are known in advance or can be obtained through measurements of samples expressing a single fluorophore. We analyzed the experimental data using non-negative least square projection, which decomposes the measured signal into a weighted sum of the individual fluorophore reference profiles. This analysis does not take into account that the local fluorophore environment or illumination conditions may cause changes in the reference profiles, which can lead to artifacts in the analysis, as were also observed here. Fully addressing such issues will require the development of analysis algorithms that can dynamically adjust the reference profiles to account for changes in probe behavior that may arise within particular (cellular) environments. Such algorithms may well be guided by minimizing the structuring observed in the residual images in order to deliver an emitter separation that accounts for the full measured signal.

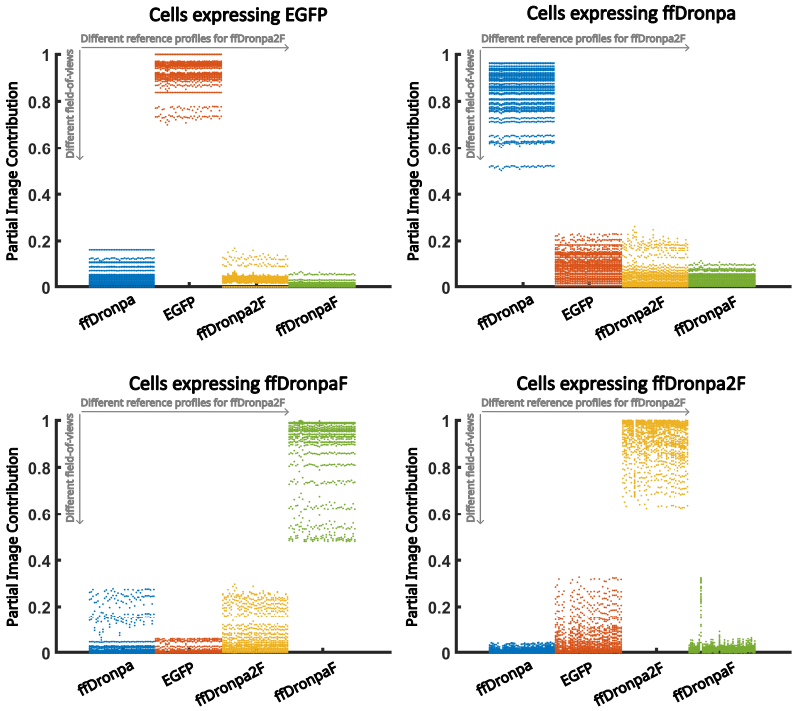

Figure 4: Influence of the reference profile on the fluorophore contribution in the exNEEMO output. Example of a contribution plot showing partial image contributions of each rsFP in the single-fluorophore datasets, where reference profiles of ffDronpa2F are varied. One vertical line is one choice of a reference profile. Data points above one another are different FOVs.

In conclusion, using exNEEMO we were able to distinguish four green rsFPs in eukaryotic cells in a per-pixel manner that maintains the full spatial resolution of the imaging. Similar to our previous work, the key advantage of the method is the ability to operate on a wide range of fluorescence dynamics since it is not limited by the temporal resolution of the detector. By providing increased multiplexing opportunities using a conceptually simple approach, our method expands the opportunities for high-content imaging in complex (biological) systems.

Acknowledgements

This work was supported by the Research Foundation-Flanders (FWO) via grants G010723N and G090819N, FLAG-ERA via grant JTC2019 Sensei, and the University of Lille via their International Chair program.

Methods

Plasmids

The fluorophores were used previously in [7] and consisted of EGFP, ffDronpa, ffDronpaF (ffDronpa K45I/F173V), and ffDronpa2F (ffDronpa K45I/M159T/F173V). These were incorporated into plasmids for expression in mammalian cells: pcDNA3-Lyn11-EGFP (with N-terminal MGCIKSKGKDSAGGGS targeting sequence), pH2B-ffDronpa (targeted to the histone H2B in the nucleus), pVimentin-ffDronpaF (targeted to the vimentin in the cell cytoskeleton) were already available in the lab. A plasmid for ffDronpa2F targeted to the peroxisome was generated by replacing EGFP with ff-Dronpa2F with C-terminal SKL sequence in the pEGFP-N1 vector.

Mammalian cell culture, transfection and fixation

HeLa cells were grown at 37°C in 5% CO_2 atmosphere in DMEM (ThermoFisher) with GlutaMAX-1 complemented with 10% fetal bovine serum (FBS) and GlutaMAX (ThermoFisher). Cells were seeded in 35-mm glass-bottom dishes (MatTek) and after 24h they were transiently transfected using X-tremeGENE HP DNA Transfection Reagent (Roche) according to the manufacturer's protocol. 24h after the transfection, cells were washed with 1x Dulbecco's phosphate-buffered saline (DPBS), pre-fixed with 4% paraformaldehyde (PFA, Electron Microscopy Sciences) solution for 2 min

at RT, washed with 1x DPBS and then the fixation was completed with 4% PFA for 12 min at RT. The prefixation step helps to preserve the native protein structures in the cells. Afterwards, cells were incubated with 10% glycine for 10 min at RT and then washed four times with 1x DPBS. Dishes with fixed cells were stored in 4°C in 1x DPBS in the dark until the imaging experiment.

Widefield image acquisition

Imaging of the fixed cells was performed on a Nikon Eclipse Ti-2 Inverted Microscope (Minato City, Japan) equipped with a 1.4 NA oil immersion objective (100× CFI Apochromat Total Internal Reflection Fluorescence) and a

ZT405/488/561/640rpcv2 dichroic mirror with a ZET405/488/561/640 nm emission filter (both Chroma Technology, Bellows Falls, Vermont) in epi-illumination. Two separate lasers at 405 and 488 nm (Oxxius, Lannion, France) were used for excitation. Images were acquired on a PCO.edge 4.2 camera (PCO, Kelheim, Germany) with an exposure time of 50 ms and optical pixel size of 78.8 nm, using varying pulses of the 405 nm light (~11 mW transmitted by the objective) in the presence of 488 nm light (~10mW transmitted by the objective). The excitation light was controlled using an Arduino-compatible microcontroller (Velleman, Gavere, Belgium). Due to the rolling-shutter readout process, the 50 ms camera exposure resulted in a maximal per-image illumination duration of 40 ms since light was applied only when all of the camera pixels were sensitive. To increase the total number of images, the images were acquired in equidistant positions over a whole dish using an automated stage loop. FOVs that were out of focus, contained emission that saturated the camera, or that did not contain any cells or that contained clearly degraded cells were excluded from the image analysis.

Image analysis

The image analysis was based on non-negative least squares projection. As was described in the text, we solve

$$\boldsymbol{D} = \boldsymbol{C}\boldsymbol{S}^{\boldsymbol{T}} + \boldsymbol{E} \tag{2}$$

for the matrix $\boldsymbol{C}$ that denotes the amount of each fluorophore in every camera pixel, given matrix $\boldsymbol{S}$ that contains the reference profiles and $\boldsymbol{E}$ an error or residual matrix that describes to what extent the calculated solution deviates from the measured values. The actual algorithm used to solve this equation is described in reference [15].

To reduce the influence of background emission on the analysis, we segmented the acquired images by calculating an average image of all four acquired images, sorting the pixel values, and choosing a threshold at the 5% cutoff level. within the disregarding pixels in the lowest 5 % of the pixel intensity range. The threshold was calculated based on the average image of all four measured frames. To correct for background, the average intensity of these disregarded pixels was then subtracted from the acquired images. The same procedure was performed to extract the reference profiles from cells that expressed just a single a single fluorophore, by calculating the average intensity seen in each image for the pixels above the threshold.

The contribution graphs in Figure 3B and elsewhere show the averaged fractional contribution of each fluorophore to the single-fluorophore reference data, and therefore act as a quality control. To calculate the fractional contribution f_i of the i-th fluorophore in a single pixel, we make use of

$$f_i = \frac{c_i b_i}{\sum_{k=1}^{4} c_k b_k} \tag{3}$$

where c_k is the contribution of the k-th fluorophore to the pixel calculated via the analysis framework, and b_k is the value of its reference profile for the fourth image. Obtaining the overall fractional contribution for a given field of view is then done by averaging f_i over all pixels over the threshold.

References

[1] Ilaria Testa, Andreas Schönle, Claas v. Middendorff, Claudia Geisler, Rebecca Medda, Christian A. Wurm, Andre C. Stiel, Stefan Jakobs, Mariano Bossi, Christian Eggeling, Stefan W. Hell, and Alexander Egner. Nanoscale separation of molecular species based on their rotational mobility. *Opt. Express*, 16(25):21093–21104, Dec 2008. doi: 10.1364/OE.16.021093. URL http://opg.optica.org/oe/abstract.cfm?URI=oe-16-25-21093.

[2] Thomas Niehörster, Anna Löschberger, Ingo Gregor, Benedikt Krämer, Hans-Jürgen Rahn, Matthias Patting, Felix Koberling, Jörg Enderlein, and Markus Sauer. Multi-target spectrally resolved fluorescence lifetime imaging microscopy. *Nature Methods*, 13(3):257–262, Mar 2016. ISSN 1548-7105. doi: 10.1038/nmeth.3740. URL https://doi.org/10.1038/nmeth.3740.

[3] Gerard Marriott, Shu Mao, Tomoyo Sakata, Jing Ran, David K. Jackson, Chutima Petchprayoon, Timothy J. Gomez, Erica Warp, Orapim Tulyathan, Holly L. Aaron, Ehud Y. Isacoff, and Yuling Yan. Optical lock-in detection imaging microscopy for contrast-enhanced imaging in living cells. *Proceedings of the National*

Academy of Sciences, 105(46):17789–17794, 2008. ISSN 0027-8424. doi: 10.1073/pnas.0808882105. URL https://www.pnas.org/content/105/46/17789.

[4] Jérôme Querard, Tal-Zvi Markus, Marie-Aude Plamont, Carole Gauron, Pengcheng Wang, Agathe Espagne, Michel Volovitch, Sophie Vriz, Vincent Croquette, Arnaud Gautier, Thomas Le Saux, and Ludovic Jullien. Photoswitching kinetics and phase-sensitive detection add discriminative dimensions for selective fluorescence imaging. *Angewandte Chemie International Edition*, 54(9):2633–2637, 2015. doi: https://doi.org/10.1002/anie.201408985. URL https://onlinelibrary.wiley.com/doi/abs/10.1002/anie.201408985.

[5] S. Duwé, W. Vandenberg, and P. Dedecker. Live-cell monochromatic dual-label sub-diffraction microscopy by mt-pcsofi. *Chem. Commun.*, 53:7242–7245, 2017. doi: 10.1039/C7CC02344H. URL http://dx.doi.org/10.1039/C7CC02344H.

[6] Daniel Wüstner. Dynamic mode decomposition of fluorescence loss in photobleaching microscopy data for model-free analysis of protein transport and aggregation in living cells, 2022. ISSN 1424-8220. URL https://doi.org/10.3390/s22134731.

[7] Hana Valenta, Siewert Hugelier, Sam Duwé, Giulia Lo Gerfo, Marcel Müller, Peter Dedecker, and Wim Vandenberg. Separation of spectrally overlapping fluorophores using intra-exposure excitation modulation. *Biophysical Reports*, 1(2):100026, Dec 2021. ISSN 2667-0747. URL https://www.sciencedirect.com/science/article/pii/S2667074721000264.

[8] Raja Chouket, Agnès Pellissier-Tanon, Aliénor Lahlou, Ruikang Zhang, Diana Kim, Marie-Aude Plamont, Mingshu Zhang, Xi Zhang, Pingyong Xu, Nicolas Desprat, Dominique Bourgeois, Agathe Espagne, Annie Lemarchand, Thomas Le Saux, and Ludovic Jullien. Extra kinetic dimensions for label discrimination. *Nature Communications*, 13(1):1482, Mar 2022. ISSN 2041-1723. doi: 10.1038/s41467-022-29172-0. URL https://doi.org/10.1038/s41467-022-29172-0.

[9] Yuling Yan, M Emma Marriott, Chutima Petchprayoon, and Gerard Marriott. Optical switch probes and optical lock-in detection (olid) imaging microscopy: high-contrast fluorescence imaging within living systems. *Biochem J*, 433(3):411–22, Feb 2011. doi: 10.1042/BJ20100992.

[10] Jung-Cheng Hsiang, Amy E Jablonski, and Robert M Dickson. Optically modulated fluorescence bioimaging: visualizing obscured fluorophores in high background. *Acc Chem Res*, 47(5):1545–54, May 2014. doi: 10.1021/ar400325y.

[11] Gerardo Abbandonato, Barbara Storti, Giovanni Signore, Fabio Beltram, and Ranieri Bizzarri. Quantitative optical lock-in detection for quantitative imaging of switchable and non-switchable components. *Microsc Res Tech*, 79(10):929–937, Oct 2016. doi: 10.1002/jemt.22724.

[12] Jérôme Quérard, Ruikang Zhang, Zsolt Kelemen, Marie-Aude Plamont, Xiaojiang Xie, Raja Chouket, Insa Roemgens, Yulia Korepina, Samantha Albright, Eliane Ipendey, Michel Volovitch, Hanna L. Sladitschek, Pierre Neveu, Lionel Gissot, Arnaud Gautier, Jean-Denis Faure, Vincent Croquette, Thomas Le Saux, and Ludovic Jullien. Resonant out-of-phase fluorescence microscopy and remote imaging overcome spectral limitations. *Nature Communications*, 8(1):969, 2017.

[13] Agnès Pellissier-Tanon, Raja Chouket, Ruikang Zhang, Aliénor Lahlou, Agathe Espagne, Annie Lemarchand, Vincent Croquette, Ludovic Jullien, and Thomas Le Saux. Resonances at fundamental and harmonic frequencies for selective imaging of sine-wave illuminated reversibly photoactivatable labels. *ChemPhysChem*, 23(23):e202200295, 2022. doi: https://doi.org/10.1002/cphc.202200295. URL https://chemistry-europe.onlinelibrary.wiley.com/doi/abs/10.1002/cphc.202200295.

[14] Katharina N Richter, Natalia H Revelo, Katharina J Seitz, Martin S Helm, Deblina Sarkar, Rebecca S Saleeb, Elisa D'Este, Jessica Eberle, Eva Wagner, Christian Vogl, Diana F Lazaro, Frank Richter, Javier Coy-Vergara, Giovanna Coceano, Edward S Boyden, Rory R Duncan, Stefan W Hell, Marcel A Lauterbach, Stephan E Lehnart, Tobias Moser, Tiago F Outeiro, Peter Rehling, Blanche Schwappach, Ilaria Testa, Bolek Zapiec, and Silvio O Rizzoli. Glyoxal as an alternative fixative to formaldehyde in immunostaining and super-resolution microscopy. *The EMBO Journal*, 37(1):139–159, 2018. doi: https://doi.org/10.15252/embj.201695709.

[15] Rasmus Bro and Sijmen De Jong. A fast non-negativity-constrained least squares algorithm. *Journal of Chemometrics: A Journal of the Chemometrics Society*, 11(5):393–401, 1997.